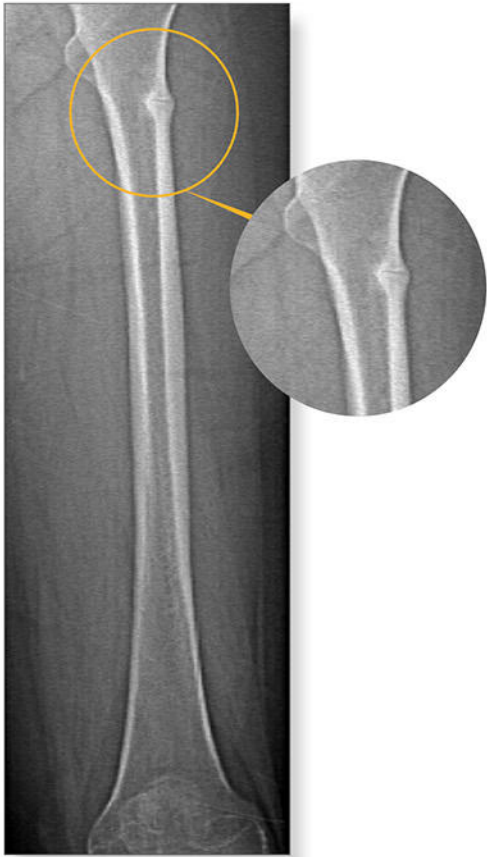


# Powerful images. **Clear answers.**



Manage Patient's concerns about  
Atypical Femur Fracture\*



Vertebral Fracture Assessment –  
a critical part of a complete  
fracture risk assessment



Advanced Body Composition<sup>®</sup>  
Assessment – the power to  
see what's inside

**Contact your Hologic rep today at [insidesales@hologic.com](mailto:insidesales@hologic.com)**

\*Incomplete Atypical Femur Fractures imaged with a Hologic densitometer, courtesy of Prof. Cheung, University of Toronto

ADS-02018 Rev 001 (9/17) Hologic Inc. ©2017 All rights reserved. Hologic, Advanced Body Composition, The Science of Sure and associated logos are trademarks and/or registered trademarks of Hologic, Inc., and/or its subsidiaries in the United States and/or other countries. This information is intended for medical professionals in the U.S. and other markets and is not intended as a product solicitation or promotion where such activities are prohibited. Because Hologic materials are distributed through websites, eBroadcasts and tradeshows, it is not always possible to control where such materials appear. For specific information on what products are available for sale in a particular country, please contact your local Hologic representative.

# NR4A1 Regulates Motility of Osteoclast Precursors and Serves as Target for the Modulation of Systemic Bone Turnover

Carina Scholtysek,<sup>1,2</sup> Natacha Ipseiz,<sup>3</sup> Christina Böhm,<sup>1,2</sup> Brenda Krishnacoumar,<sup>1,2</sup> Martin Stenzel,<sup>1,2</sup> Tina Czerwinski,<sup>4</sup> Katrin Palumbo-Zerr,<sup>1,2</sup> Tobias Rothe,<sup>1,2</sup> Daniela Weidner,<sup>1,2</sup> Alexandra Klej,<sup>1,2</sup> Cornelia Stoll,<sup>1,2</sup> Jörg Distler,<sup>1</sup> Jan Tuckermann,<sup>5</sup> Martin Herrmann,<sup>1</sup> Ben Fabry,<sup>4</sup> Wolfgang H Goldman,<sup>4</sup> Georg Schett,<sup>1</sup> and Gerhard Krönke<sup>1,2</sup>

<sup>1</sup>Department of Internal Medicine 3, University of Erlangen-Nuremberg, Erlangen, Germany

<sup>2</sup>Nikolaus Fiebiger Center of Molecular Medicine, University of Erlangen-Nuremberg, Erlangen, Germany

<sup>3</sup>School of Medicine, University of Cardiff, Cardiff, Wales

<sup>4</sup>Department of Biophysics, University of Erlangen-Nuremberg, Erlangen, Germany

<sup>5</sup>Institute of Comparative Molecular Endocrinology, University of Ulm, Ulm, Germany

## ABSTRACT

NR4A1 (Nur77 or NGFI-B), an orphan member of the nuclear receptor superfamily, has been identified as a key regulator of the differentiation and function of myeloid, lymphoid, and mesenchymal cells. The detailed role of NR4A1 in bone biology is incompletely understood. Here, we report a role for NR4A1 as novel factor controlling the migration and recruitment of osteoclast precursors during bone remodeling. Myeloid-specific but not osteoblast-specific deletion of NR4A1 resulted in osteopenia due to an increase in the number of bone-lining osteoclasts. Although NR4A1-deficient osteoclast precursors displayed a regular differentiation into mature osteoclasts, they showed a hyper-motile phenotype that was largely dependent on increased osteopontin expression, suggesting that expression of NR4A1 negatively controlled osteopontin-mediated recruitment of osteoclast precursors to the trabecular bone. Pharmacological activation of NR4A1, in turn, inhibited osteopontin expression and osteopontin-dependent migration of osteoclast precursors resulted in reduced abundance of bone-resorbing osteoclasts *in vivo* as well as in an ameliorated bone loss after ovariectomy in mice. This study identifies NR4A1 as a crucial player in the regulation of osteoclast biology and bone remodeling and highlights this nuclear receptor as a promising target for therapeutic intervention during the treatment of osteoporosis. © 2018 The Authors. *Journal of Bone and Mineral Research* Published by Wiley Periodicals Inc.

**KEY WORDS:** OSTEOCLASTS; CELL MIGRATION; NUCLEAR RECEPTORS; OSTEOPOROSIS; OSTEOIMMUNOLOGY

## Introduction

Bone continuously undergoes remodeling throughout life to adapt its structure in response to damage and changing biomechanical conditions. This dynamic process involves the coordinated action of bone-forming osteoblasts and bone-resorbing osteoclasts (OCs). OC differentiation, in turn, depends on a series of regulatory steps, which includes proliferation and directed migration of myeloid osteoclast precursors (OCPs) as well as their fusion into mature multinucleated OCs that subsequently initiate osteoclastic bone resorption.<sup>(1,2)</sup> Increased OC activity results in accelerated bone turnover and pathological bone loss, which is regularly observed during diseases such as rheumatoid arthritis and different forms of osteoporosis.<sup>(3)</sup>

Although our understanding of the molecular events underlying OC differentiation and fusion has steadily expanded over the past two decades, less is known about mechanisms that control the directed recruitment and migration of OCPs and OCs to the bone surface and areas of bone resorption, respectively.

Nuclear receptors represent ligand-activated transcription factors that act as master regulators of lipid and glucose metabolism.<sup>(4,5)</sup> Whereas for the subgroup of steroid hormone receptors a role in the immune response and bone metabolism is well established, the role of adopted orphan receptors is just emerging. Adopted orphan nuclear receptors were shown to control the innate and adaptive immune response<sup>(6,7)</sup> and act as crucial factors during bone homeostasis.<sup>(8–12)</sup> NR4A1 (Nur77) is an orphan nuclear receptor and, together with NR4A2 (Nurr1) and

This is an open access article under the terms of the Creative Commons Attribution License, which permits use, distribution and reproduction in any medium, provided the original work is properly cited.

Received in original form January 29, 2018; revised form May 29, 2018; accepted June 21, 2018. Accepted manuscript online June 27, 2018.

Address correspondence to: Carina Scholtysek, PhD, Department of Internal Medicine 3, University of Erlangen-Nuremberg, Glückstraße 6, Erlangen 91054, Germany  
E-mail: carina.scherbel@uk-erlangen.de

Additional Supporting Information may be found in the online version of this article.

*Journal of Bone and Mineral Research*, Vol. 33, No. 11, November 2018, pp 2035–2047

DOI: 10.1002/jbmr.3533

© 2018 The Authors. *Journal of Bone and Mineral Research* Published by Wiley Periodicals Inc.

NR4A3 (NOR-1), constitutes the NR4A subfamily of nuclear receptors.<sup>(13)</sup> NR4A family members seem to be primarily regulated at the transcriptional and posttranslational level and are rapidly induced in response to stimuli such as LPS and oxidized lipids.<sup>(14,15)</sup> These nuclear receptors are widely expressed in myeloid, lymphoid, as well as mesenchymal and epithelial cells and have been implicated as important coordinators for the differentiation of regulatory T cells, Ly6C<sup>low</sup> monocytes, thymic macrophages, as well as regulators of energy homeostasis and muscle mass.<sup>(16–19)</sup> NR4A1 was recently suggested to exert a suppressive activity during OC differentiation and NR4A1-deficient mice were shown to display an osteopenic phenotype.<sup>(20)</sup> However, it remains to be elucidated how this nuclear receptor controls bone homeostasis in vivo and which cell types and mechanism are involved and responsible for this phenotype.

Here, we show that myeloid-specific, but not osteoblast-specific, deletion of NR4A1 resulted in osteopenia that was paralleled by an increased accumulation of OCs at the trabecular bone surface. Mechanistically, NR4A1 controlled the expression of genes involved in the motility of OCPs such as osteopontin (OPN) but did not directly impact on OC differentiation or fusion. Accordingly, ligand-induced activation of NR4A1 ameliorated OCP motility and OC accumulation within the trabecular bone and protected mice against bone loss in the ovariectomy (OVX)-induced model of postmenopausal osteoporosis. The results of the presented study highlight the therapeutic potential of the nuclear receptor for the treatment of osteoporosis and bone-related diseases.

## Materials and Methods

### Mice

All mice were maintained at the specific pathogen-free animal care facility (FPZ) of the University of Erlangen-Nuremberg and housed in a room at 23 ± 2°C, with 50 ± 10% humidity and a 12-hour light/dark cycle (lights on from 8:00 a.m. to 8:00 p.m.). All mice were allowed free access to water and regular rodent chow. All animal experiments were approved by the government of Unterfranken, Germany. Mice with floxed NR4A1 allele exon 4 (Nr4a1<sup>fl/fl</sup>) were a gift from Professor Pierre Chambon, Institute for Genetics and Molecular and Cellular Biology, Illkirch-Graffenstaden, France. To obtain conditional deletion in myeloid cells, NR4A1<sup>fl/fl</sup> mice were crossed to mice expressing Cre recombinase driven by *Lysozyme M* promoter (LysMCre; 004781, Jackson Laboratory, Bar Harbor, ME, USA) to achieve NR4A1<sup>fl/fl</sup>/LysMCre(+/-) conditional knockouts and analyzed with wild-type littermates (NR4A1<sup>fl/fl</sup>/LysMCre(-/-)) used as controls. For conditional deletion of NR4A1 in osteoblasts, NR4A1<sup>fl/fl</sup> mice were crossed to Runx2Cre(+/-) (MGI, 4455015) mice, which were a gift from Jan Tuckermann, Institute of Comparative Molecular Endocrinology, University of Ulm, Germany. Additionally, we used for experiments NR4A1 knockout mice (Nr4a1<sup>-/-</sup>; 006187, Jackson Laboratory) and C57BL/6JRj wild-type mice as controls (NR4A1+/+; Janvier Labs, Le Genest St Isle, France).

### Ovariectomy

Female C57BL/6JRj wild-type mice were obtained from Janvier Labs and experiments were performed according to guidelines of laboratory animal care and use. All efforts were made to reduce the number of animals tested and their suffering. For ovariectomy, mice (12 weeks of age) were anesthetized with a ketamine-xylazine (KX) solution and bilaterally ovariectomized, while ovaries of the sham group were left intact. Two weeks after

ovariectomy, we started treatment to ensure the development of osteoporosis in all mice. Mice were divided into four groups: sham-operated mice (sham, *n* = 6), OVX mice (control, *n* = 5), Cytosporone B (C2997 Sigma)-treated OVX mice (10 mg/kg body weight in DMSO, *n* = 4), and Cytosporone B (C2997 Sigma, St. Louis, MO, USA)-treated sham-operated mice (10 mg/kg body weight in DMSO, *n* = 6). Mice were weighed weekly and concentrations were calculated for the Cytosporone B administration for 6 weeks. The animals of each group were intraperitoneally injected with the NR4A1 agonist or the vehicle (DMSO), respectively. Feed consumption and body weight were monitored weekly for 6 weeks. No adverse effects were detected. All mice were killed after 6 weeks of treatment at the age of 20 weeks. One tibia was excised for histological analyses and one for  $\mu$ CT imaging. For immunofluorescence and the real-time analysis of NR4A1 expression, female C57BL/6JRj wild-type mice were obtained from Janvier Labs and ovariectomized at the age of 12 weeks. For this, ovariectomy, mice were anesthetized with a ketamine-xylazine (KX) solution and bilaterally ovariectomized, while ovaries of the sham group were left intact. The ovariectomized mice were allowed to recover for 2 weeks to ensure the development of osteoporosis. Mice were divided into two groups: sham-operated mice (sham, *n* = 4) and OVX mice (control, *n* = 4). One tibia was used for immunofluorescence (cyrosections) and one for real-time analysis.

### Micro-computed tomography imaging ( $\mu$ CT)

Tibial bones were fixed in 4% paraformaldehyde overnight before the analyses. All  $\mu$ CT imaging was performed using the cone-beam Desktop Micro Computer Tomograph “ $\mu$ CT 40” by SCANCO Medical AG (Bruttisellen, Switzerland; <http://www.scanco.ch/en/systems-solutions/specimen/microct40.html>). The settings were optimized for calcified tissue visualization at 55 kVp at a current of 145  $\mu$ A and 200 ms integration time for 500 projections/180°. For the segmentation of 3D-volumes, an isotropic voxel size of 8.4  $\mu$ m, and an evaluation script with adjusted grayscale thresholds of the operating system “Open VMS” by SCANCO Medical was used. For 3D- $\mu$ CT analysis, measurements were conducted 1680  $\mu$ m around 400  $\mu$ m below the approximate middle of growth plate, left or right of the tibia metaphysis.

### Cell culture

Bone marrow-derived monocytes (BMMs) were isolated as previously described and differentiated into osteoclast precursors (OCPs), mature osteoclasts (OCs), or bone marrow-derived macrophages (BMDMs).<sup>(8)</sup> Briefly, hematopoietic bone marrow cells were purified from tibial bone with a 70- $\mu$ m cell strainer, cultured overnight, and stimulated with appropriate growth medium (MEM Alpha Medium 1 × GlutaMAX, GIBCO; #32571-028, containing 10% L929 conditioned medium, 10% FCS, and 1% penicillin/streptomycin) at 37°C and 5% CO<sub>2</sub>. OCPs were cultured in OC-growth medium (MEM Alpha Medium 1 × GlutaMAX, GIBCO; #32571-028, containing 10% L929 conditioned medium, 10 ng/mL RANKL, 10% FCS, and 1% penicillin/streptomycin) for 24 hours. To generate mature multinucleated osteoclasts (OCs), cells were cultured in OC-growth medium (MEM Alpha Medium 1 × GlutaMAX, GIBCO; #32571-028, containing 10% L929 conditioned medium, 10 ng/mL RANKL, 10% FCS, and 1% penicillin/streptomycin) for 72 hours. To obtain BMDMs, BMMs were incubated with growth medium (MEM

Alpha Medium 1× GlutaMAX, GIBCO; #32571-028, containing 10% L929 conditioned medium, 10% FCS, and 1% penicillin/streptomycin) for 5 days and then seeded for experiments. Osteoclast differentiation was quantified by counting multinucleated (>3 nuclei) TRAP+ cells on day 4 of OC culture. Osteoclast fusion events were quantified by counting the nuclei per osteoclast. For analysis of osteoclast resorption, osteoclast differentiation was conducted in OsteoLyse assay kit (Lonza, Basel, Switzerland) and osteoclast resorption activity was quantified by calcium release from bone into culture medium.

#### In vitro scratch assay

Horizontal migration analysis via in vitro scratch assay was performed as previously described.<sup>(21)</sup> Briefly, BMMs were seeded into 6-cm dishes and incubated overnight in OC-growth medium allowing cells to adhere and spread on the substrate completely. Cell monolayer was scraped in a straight line with a cell scraper to create an empty half of the well. Subsequently, cells were washed five times with growth medium to remove floating cells. Cells were allowed to migrate back into the scratched area for 24 hours and stained with crystal violet solution (HT90132 Sigma) and counted.

#### Transwell migration assay

To analyze vertical migration activity, we used transwell migration chambers (Corning, Berlin, Germany). OCPs were seeded in the upper chamber with OC-growth medium. Cells were allowed to migrate through a polycarbonate filter (8- $\mu$ m pore size) for 8 hours. Non-migrated cells in the upper chamber were removed with a cotton swab. Migrated cells on the lower side of the insert were fixed and stained with crystal violet, counted, and quantified using a Zeiss Axioskop 2 (Carl Zeiss, Jena, Germany) microscope equipped with a digital camera and image analysis system (Osteomeasure; Osteometrics, Decatur, GA, USA).

#### Chromatin immunoprecipitation (ChIP) assays

ChIP assays were performed using the ChIP-IT Express Kit (53008; Active Motif, Carlsbad, CA, USA). An amount of 20  $\mu$ g sonicated chromatin extract was incubated with antibodies against NR4A1 (13851; Abcam, Cambridge, MA, USA) or normal rabbit IgG antibodies (no. sc-2027, Santa Cruz Biotechnology, Dallas, TX, USA). After purification of DNA, bound sequences were determined by quantitative real-time PCR.

#### Adenovirus constructs and gene transduction in vitro

For NR4A1 gene overexpression, mouse NR4A1 adenovirus (ADV-266056; Vector Biolabs, Malvern, PA, USA) and for control GFP adenovirus (1060; Vector Biolabs) were used. OCPs were incubated with growth medium containing the NR4A1 adenovirus (multiplicity of infection = MOI of 1000) for 24 hours at 37°C. After 24 hours, the medium was changed. Experiments were performed 48 hours after transduction. Adenovirus transduction efficiency in terms of working MOI was established by titrating NR4A1 and GFP adenovirus on OCPs before.

#### Histology

For histomorphometric analysis, tibial bones were fixed overnight in 4% formalin. For osteoclast analysis, tibial bones

were decalcified in 14% EDTA for 2 weeks until the bone was flexible. Serial paraffin sections (2  $\mu$ m) from tibias were cut and stained with tartrate-resistant acid phosphatase (TRAP) by using a leukocyte acid phosphatase staining kit (Sigma; 387A) for detection of multinucleated osteoclasts (TRAP+ cells). Measurements were taken beginning at a standard point in the tibia below the growth plate at the end of primary spongiosa, including an area of 3-mm secondary spongiosa. Histomorphometric analysis was taken from three sections per mouse and three mice for each genotype. Quantification of osteoblasts was performed on methacrylate-embedded undecalcified plastic sections stained with Goldner's stain for bone. Analysis of all bone parameters were quantified with the use of a Zeiss Axioskop 2 microscope equipped with a digital camera and image analysis system (Osteomeasure; Osteometrics).

#### TUNEL assay

For determination of apoptosis, deparaffinized, ethanol-dehydrated bone sections were stained using the in situ Cell Death Detection Kit (11684795910; Roche, Mannheim, Germany) according to the manufacturer's protocol. Nuclei were counterstained with DAPI mounting solution (Vector Laboratories, Burlingame, CA, USA).

#### ELISA

Blood from mice was collected by retro-orbital bleeding starved for overnight. To collect serum, blood was collected with heparinized micro-hematocrit capillary tubes transferred to BD Microtainer SST tubes, and blood samples were then inverted five times and remained at room temperature for 30 minutes to allow clotting before centrifugation for 5 minutes at 4°C.

Serum levels of OPN (MOST00; R&D Systems, Minneapolis, MN, USA) were measured according to the instructions of the manufacturer's protocol. To determine the systemic levels of bone-related degradation products derived from C-terminal telopeptides of type I collagen (RatLaps; CTX-I) serum levels of RatLaps CTX-I (AC-06F1; IDS, Boldon, UK) were measured according to the instructions of the manufacturer.

#### Western blot analysis

Proteins were separated by SDS-PAGE and transferred to a polyvinylidene difluoride membrane (PVDF). The membrane was incubated with the appropriate primary antibody and HRP-conjugated secondary antibodies (Dako, Glostrup, Denmark) (Table 1). Blots were visualized using enhanced chemiluminescence (ECL).  $\beta$ -actin(A5441, Sigma-Aldrich) or Lamin B1 (133741; Abcam) was used as a loading control.

#### RT-PCR analysis

Total RNA was isolated from cells and bone using peqGOLD TRIFast (peqlab, Erlangen, Germany). An amount of 1  $\mu$ g was used for the first-strand complementary DNA synthesis

**Table 1. Primary Antibodies**

Primary antibody	Catalog no.	Company
OPN	8448	Abcam
Nfatc1	7294	Santa Cruz
NR4A1	153914	Abcam

(Amersham Biosciences, GE Healthcare, Little Chalfont, UK), which was then used for SYBR green-based quantitative RT-PCR as described previously.<sup>(22)</sup> Triplicates were performed according to the manufacturer's instructions. The RT-PCR primer sequences used are shown in Table 2.

### Immunofluorescence staining

Four percent PFA-fixed, 0.25% Triton X-100-permeabilized cells were stained with appropriate primary antibodies. HRP or Alexa Fluor-conjugated antibodies (Life Technologies, Darmstadt, Germany) were used as secondary antibodies. Osteoclasts were visualized with Alexa Fluor 488 dye phalloidin (Thermo Fisher Scientific, Waltham, MA, USA; #A12379, dilution 1:400) and osteopontin (R&D Systems, #AF808, dilution 1:400). In addition, cell nuclei were stained using DAPI (Roche, dilution 1:3000). Stained cells were visualized using a Nikon Eclipse 80i microscope (Nikon, Tokyo, Japan). For immunofluorescence on bone sections, tibia of ovariectomized or sham-operated wild-type mice were collected and fixed o.n. in 4% PFA. Bone was decalcified for 7 days in decalcification buffer (4°C) and subsequently incubated o.n. in 30% sucrose (RT). The frozen samples (Tissue-Tek O.C.T.) were cut in 7-µm cryosections and used for immunofluorescence. Sections were blocked with 0.2% BSA and 0.1% Saponin in PBS (BSA: Carl Roth, Karsruhe, Germany, #9638.1; Saponin: Sigma-Aldrich, #84510) and incubated with primary rabbit-anti Nr4a1 antibody (Abcam, #ab13851, dilution 1:100) o.n. at 4°C. In addition cell nuclei were stained with DAPI (Roche, dilution 1:3000) and cytoskeleton was stained with Phalloidin (Alexa Flour 647, Thermo Fisher #A22287, dilution 1:50). Immunofluorescence was analyzed using a confocal microscope (Leica TCS SP5 II, Ex: 633 nm / Det: 650-670 nm).

### Statistical analysis

Statistical analyses were performed using GraphPad Prism software (GraphPad Software, Inc., La Jolla, CA, USA). Results are depicted as median ± interquartile range (IQR), if not stated otherwise. For a two-group comparison, a Student's *t* test was applied, if the pretest for normality (D'Agostino-Pearson normality test) was not rejected at the 0.05 significance level;

otherwise, a Mann-Whitney *U* test for nonparametric data was used. Any *p* values less than 0.05 were considered significant. Results are expressed as mean ± SE (SEM). No statistical method was used to pre-determine the sample size.

## Results

### Deletion of NR4A1 in osteoblasts does not affect bone homeostasis

To elucidate a role of NR4A1 during bone homeostasis, we generated mice carrying different cell type-specific deletions of NR4A1. Initially, we crossed NR4A1-floxed mice (NR4A1<sup>fl/fl</sup>) with Runx2-Cre mice<sup>(23)</sup> to achieve a conditional deletion of NR4A1 in mesenchymal progenitors of osteoblasts (NR4A1<sup>fl/fl</sup>Runx2Cre (+/-)). In addition, we generated mice carrying a deletion of this nuclear receptor in myeloid cells by crossing NR4A1-floxed mice with LysM-Cre mice.<sup>(24)</sup> Micro-computed tomography (µCT) analysis of the skeletal phenotype of female NR4A1<sup>fl/fl</sup>Runx2Cre (+/-) conditional knockout mice and their wild-type littermates (NR4A1<sup>fl/fl</sup>Runx2Cre(-/-) did not reveal significant changes in the trabecular bone parameters bone volume to total volume, bone mineral density, trabecular number, trabecular thickness, or trabecular separation (Fig. 1A, B). Likewise, we observed no difference in the cortical parameters (cortical thickness and moment of inertia) between female NR4A1<sup>fl/fl</sup>Runx2Cre (+/-) mice and their wild-type littermates (Fig. 1C). Also, the histomorphometric analysis of tibial bones showed no difference in the percentage of trabecular bone surface covered by osteoblasts or in the number of osteoblasts per bone surface (Fig. 1D). Because the activation state of osteoblasts and osteocytes directly impacts on the differentiation of OCs, we additionally quantified the percentage of surface covered by OCs and the number of OCs per bone surface, both of which were unaltered in NR4A1<sup>fl/fl</sup>Runx2Cre (+/-) mice and their wild-type littermates (Fig. 1E).

### NR4A1 expression in myeloid cells restricts the number of OCs within trabecular bone

In contrast, LysM-Cre-driven deletion of NR4A1 resulted in sufficient deletion of this nuclear receptor in osteoclasts (Supplemental Fig. S1A) as well as in osteopenia in NR4A1<sup>fl/fl</sup>LysMCre (+/-) in

**Table 2.** RT-PCR Primer Sequences

Primer	Forward sequence	Reverse sequence
NR4A1	CGGACAGACAGCCTAAAAGG	TAACGTCCAGGGAACAGAG
NR4A2	GACCGGCTCTATGGAGATCA	ACCCATTGCAAAGATGAG
NR4A3	TCAGCCTTTTTGGAGCTGTT	TAACCCAGITTCGCTCTGTGA
OPN	ACTTGTGGCTCTGATGTTC	TCACCATTCCGGATGAGTCTG
CD44	GCAAGAGGCAAAGTCCCCAAGCTGT	CCAAGCTGTGTGCCACAAAACCTTG
Itgb3	TTGAGTGTGGGGTGTGCCGC	GCCCATGGCCGGAACACATCT
c-src	CGTGGCTGTACCAAGGACCC	TGGTGCTTTCCCGCACGAGG
RAC1	CCAATACTCCTATCATCCTCG	CAGCAGCATTCTCTTCC
RAC2	CCAGCACCCCATCATCCTGG	GGGCGCTTCTGCTGTCGTGTG
VEGFR2	CATCACCGAGAACAAGAACA	CATTGATCTTGCCTCACAG
CXCR4	TGCAGCAGGTAGCAGTGA	TGTATATACTCACACTGATCGGTT
VCAM1	GCTATGAGGATGGAAGACTCTGG	ACTTGTGCAGCCACCTGAGATC
Actr2	GCGGGGACTTCCGGTTT	ACTTCACAAACCCAGTGCCG
ICAM1	AAACCAGACCCTGGAAGTGCAC	GCCTGGCATTTCAGAGTCTGCT
IGF1	GTGGATGCTTTCAGTTCGTGTG	TCCAGTCTCCTCAGATCACAGC
S1PR1	ACTACACAACGGGAGCAACAG	GATGGAAAGCAGGAGCAGAG
β-actin	TGTCCACCTTCCAGCAGATGT	AGCTCAGTACAGTCCGCCTAGA

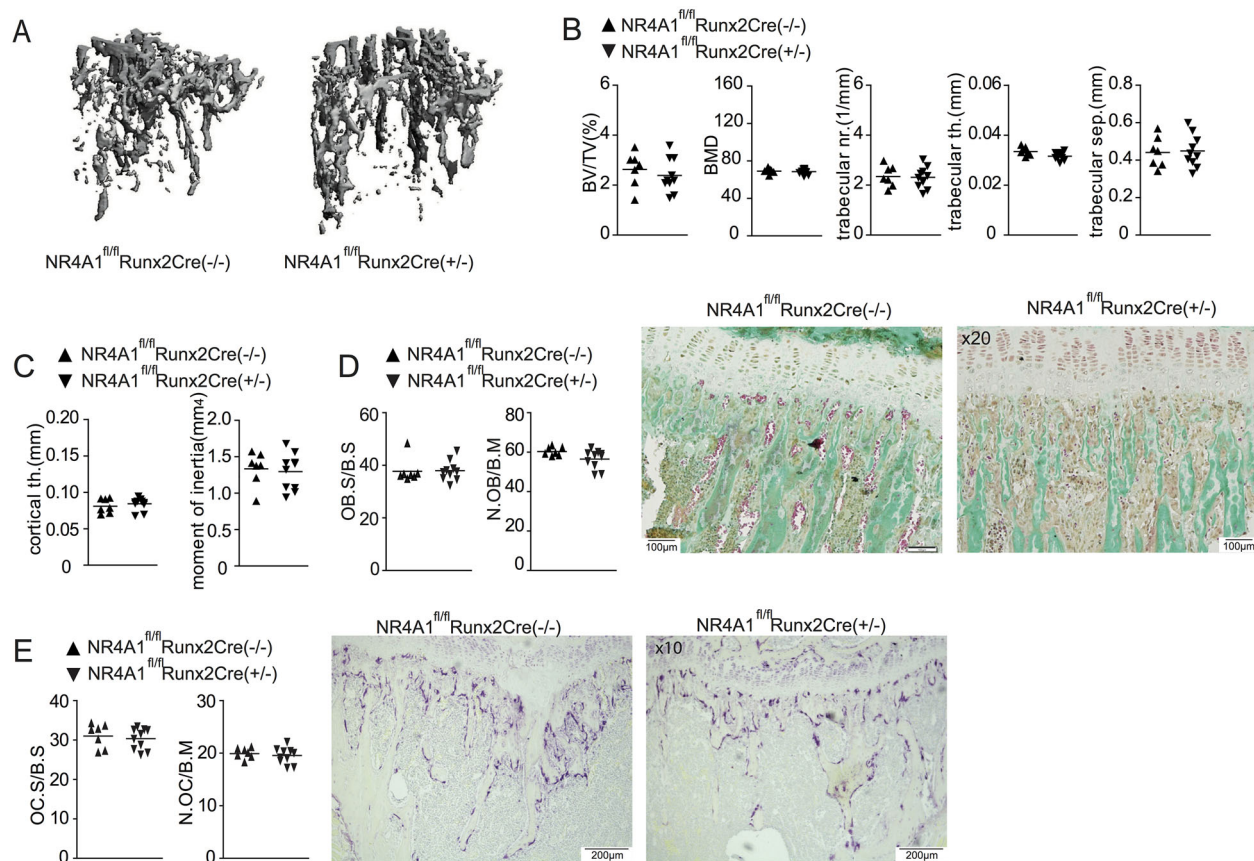


**Fig. 1.** NR4A1 deficiency in osteoblasts does not affect bone parameters. (A)  $\mu$ CT images of the skeletal phenotype of female NR4A1<sup>fl/fl</sup>Runx2Cre(+/-) and their wild-type littermates (NR4A1<sup>fl/fl</sup>Runx2Cre(-/-)) at 12 weeks of age. (B)  $\mu$ CT analysis of trabecular bone parameters of tibial bone including the fraction of bone volume to total volume (BV/TV), bone mineral density (BMD), trabecular number (trabecular nr.), trabecular thickness (trabecular th.), and trabecular separation (trabecular sep.). (C)  $\mu$ CT analysis of cortical bone parameters of tibial bone including the fraction of cortical thickness (cortical th.) and moment of inertia. (D) Histomorphometric analysis by Goldner staining of the number of osteoblasts per bone surface (N.OB/B.M) and the percentage of surfaces covered by osteoblasts (OB.S/B.S) in NR4A1<sup>fl/fl</sup>Runx2Cre(+/-) conditional knockouts compared with their wild-type littermates. (E) Histomorphometric analysis by TRAP staining of the number of osteoclasts per bone surface (N.OB/B.M) and the percentage of surfaces covered by osteoblasts (OB.S/B.S) in NR4A1<sup>fl/fl</sup>Runx2Cre(+/-) conditional knockouts compared with their wild-type littermates.

comparison to their wild-type littermates (NR4A1<sup>fl/fl</sup>LysMCr(-/-)) (Fig. 2A, B). This phenotype was characterized by a decreased bone volume to total volume, decreased bone mineral density, as well as decreased trabecular number and spacing between NR4A1<sup>fl/fl</sup>LysMCr(+/-) and their wild-type littermates. The cortical bone parameters revealed no changes between both groups of mice (Fig. 2C).

Histomorphometric analysis of tibial cancellous bone showed no differences in osteoblast parameters in NR4A1<sup>fl/fl</sup>LysMCr(+/-) and their wild-type littermates (Fig. 1D), which largely excluded an indirect effect of myeloid-specific NR4A1 deletion on bone formation. Likewise, we did not observe an altered number of TUNEL-positive apoptotic cells in bone sections of these mice (Supplemental Fig. S1B). Numbers of OCs per bone surface and the percentage of surfaces covered by OCs, in turn, were significantly increased when compared with wild-type littermates (Fig. 2E), indicating that the observed osteopenic phenotype resulted from increased abundance of OCs. Measurement of the concentrations of bone-related degradation products derived from C-terminal telopeptides of type I collagen (RatLaps; CTX-I) in the sera of the respective mice revealed an elevation of bone resorption in

NR4A1<sup>fl/fl</sup>LysMCr(+/-) mice, which is suggestive of increased osteoclastic activity (Fig. 2F). Taken together, our data confirmed a role of NR4A1 in bone turnover and suggested that this nuclear receptor acted as an intrinsic factor controlling the recruitment, fusion, or differentiation of myeloid OCPs and OCs, respectively.

#### NR4A1 expression does not influence osteoclast differentiation

To evaluate a potential role of NR4A1 in OC differentiation, we determined expression of this nuclear receptor in OCPs and OCs. NR4A1 was induced by RANKL in OCPs in a concentration-dependent manner (Fig. 3A). Likewise, we detected high expression of NR4A1 mRNA and protein during early stages of OCPs (day 1) (Fig. 3B, C). To our surprise, analysis of OC differentiation from wild-type and NR4A1 bone marrow cells showed that NR4A1<sup>-/-</sup> OCPs underwent regular differentiation into multinucleated OCs, which included a regular expression of an OC-specific transcriptional signature and thus excluded a major role of NR4A1 during this differentiation process (Fig. 3D, E). In line with this finding, measurement of bone resorption

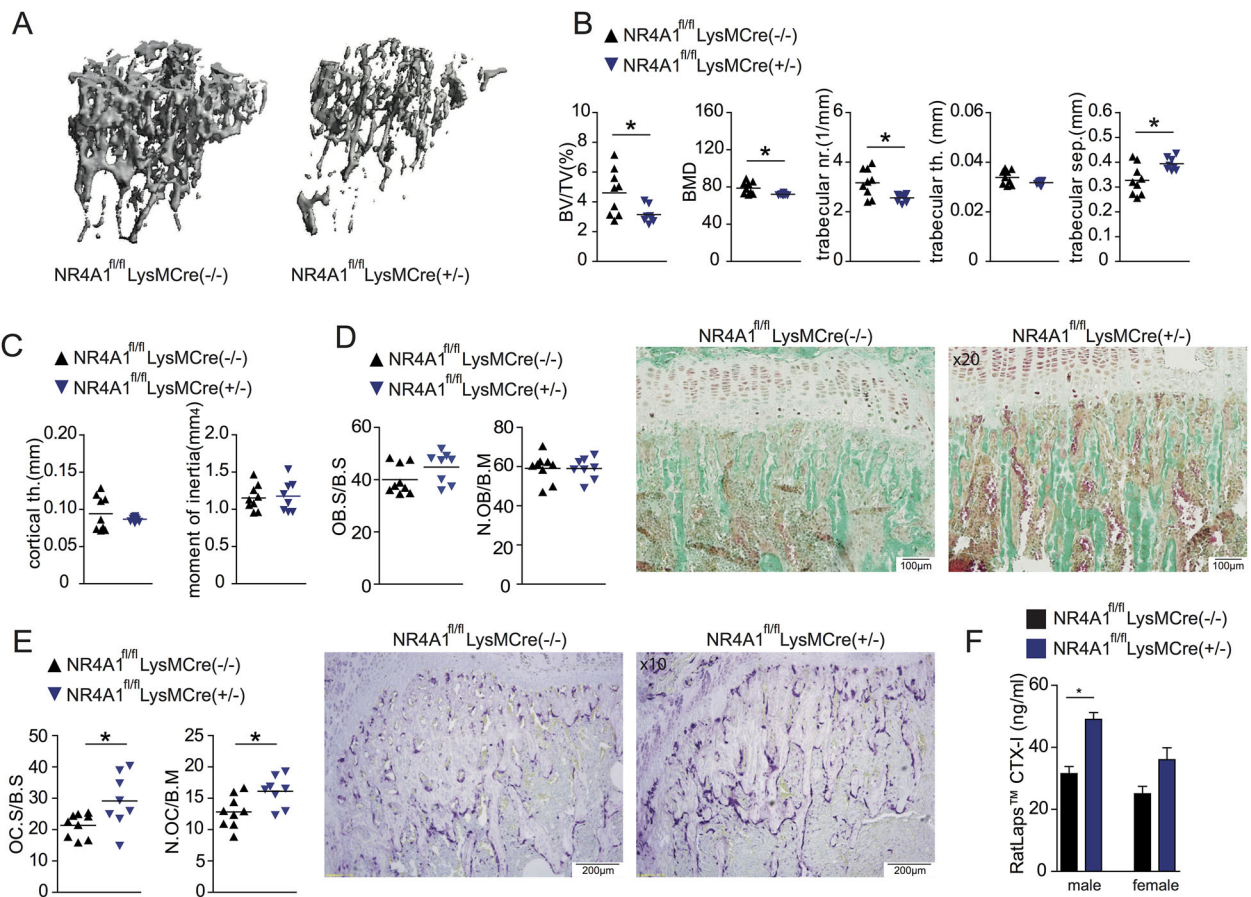


**Fig. 2.** NR4A1-mediated regulation of bone homeostasis by myeloid cells. (A)  $\mu$ CT images of the skeletal phenotype of female NR4A1<sup>fl/fl</sup>LysMCre(+/-) and their wild-type littermates (NR4A1<sup>fl/fl</sup>LysMCre(-/-)) at 12 weeks of age. (B)  $\mu$ CT analysis of trabecular bone parameters of tibial bone including bone volume to trabecular volume (BV/TV), bone mineral density (BMD), trabecular number (trabecular nr.), trabecular thickness (trabecular th.), and trabecular separation (trabecular sep.). (C)  $\mu$ CT analysis of cortical bone parameters of tibial bone including cortical thickness (cortical th.) and moment of inertia. (D) Histomorphometric analysis by Goldner staining of the number of osteoblasts per bone surface (N.OB/B.M) and the percentage of surfaces covered by osteoblasts (OB.S/B.S) in NR4A1<sup>fl/fl</sup>LysMCre(+/-) conditional knockouts compared with their wild-type littermates. (E) Histomorphometric analysis by TRAP staining of the number of osteoclasts per bone surface (N.OC/B.M) and the percentage of surfaces covered by osteoclasts (OB.S/B.S) in NR4A1<sup>fl/fl</sup>LysMCre(+/-) conditional knockouts compared with their wild-type littermates. (F) Measurement of serum crosslaps of male and female NR4A1<sup>fl/fl</sup>LysMCre(+/-) conditional knockouts and wild-type mice at 12 weeks of age.

revealed no difference in the bone-resorption capacity of WT and NR4A1<sup>-/-</sup> OCPs (Fig. 3F). All these experiments were reproduced with bone marrow cells derived from mice carrying a constitutive and a LysM-Cre-driven deletion of NR4A1, both of which yielded similar results (Supplemental Fig. S2A–C). Likewise, we did not observe a changed expression or nuclear localization of Nfatc1, a key transcription factor of osteoclast differentiation, in Nr4a1-deficient osteoclasts (Supplemental Fig. S2D). An immunofluorescence-based analysis also showed a regular fusion capacity of wild-type and NR4A1<sup>-/-</sup> OCPs (Fig. 3G, H). However, NR4A1<sup>-/-</sup> OCPs displayed a significantly increased number in lamellipodia (indicated by orange arrows; Fig. 3F, I), potentially indicating a hypermotile phenotype in these cells.

#### NR4A1 regulates the migratory activity of osteoclast precursors

We consequently evaluated a potential role for NR4A1 in the regulation of OCP migration and performed transwell as well as in vitro scratch-assays to quantify the migratory activity of wild-type

and NR4A1<sup>-/-</sup> OCPs. Indeed, NR4A1-deficient OCPs showed a stronger vertical and horizontal migration activity during transwell migration experiments and during in vitro scratch-assays, respectively (Fig. 4A, B). RANKL administration increased the motility of OCPs and resulted in an exacerbated migratory activity of NR4A1<sup>-/-</sup> OCPs (Fig. 4B). These data suggested that the presence of NR4A1 exerted an inhibitory influence on OCP migration. Accordingly, we observed that addition of Cyclosporine B (CytoB), a naturally occurring agonist of NR4A1,<sup>(25)</sup> inhibited cell migration of wild-type but not of NR4A1<sup>-/-</sup> OCPs (Fig. 4B). In line with these data, we observed that adenovirus-mediated overexpression of NR4A1 also blocked OCP migration and completely rescued the hypermotile phenotype of NR4A1<sup>-/-</sup> OCPs (Fig. 4C).

#### NR4A1 acts as transcriptional repressor of the motility of osteoclast precursors

To identify mechanisms underlying the NR4A1-mediated control of OCP motility, we performed a gene expression analysis in

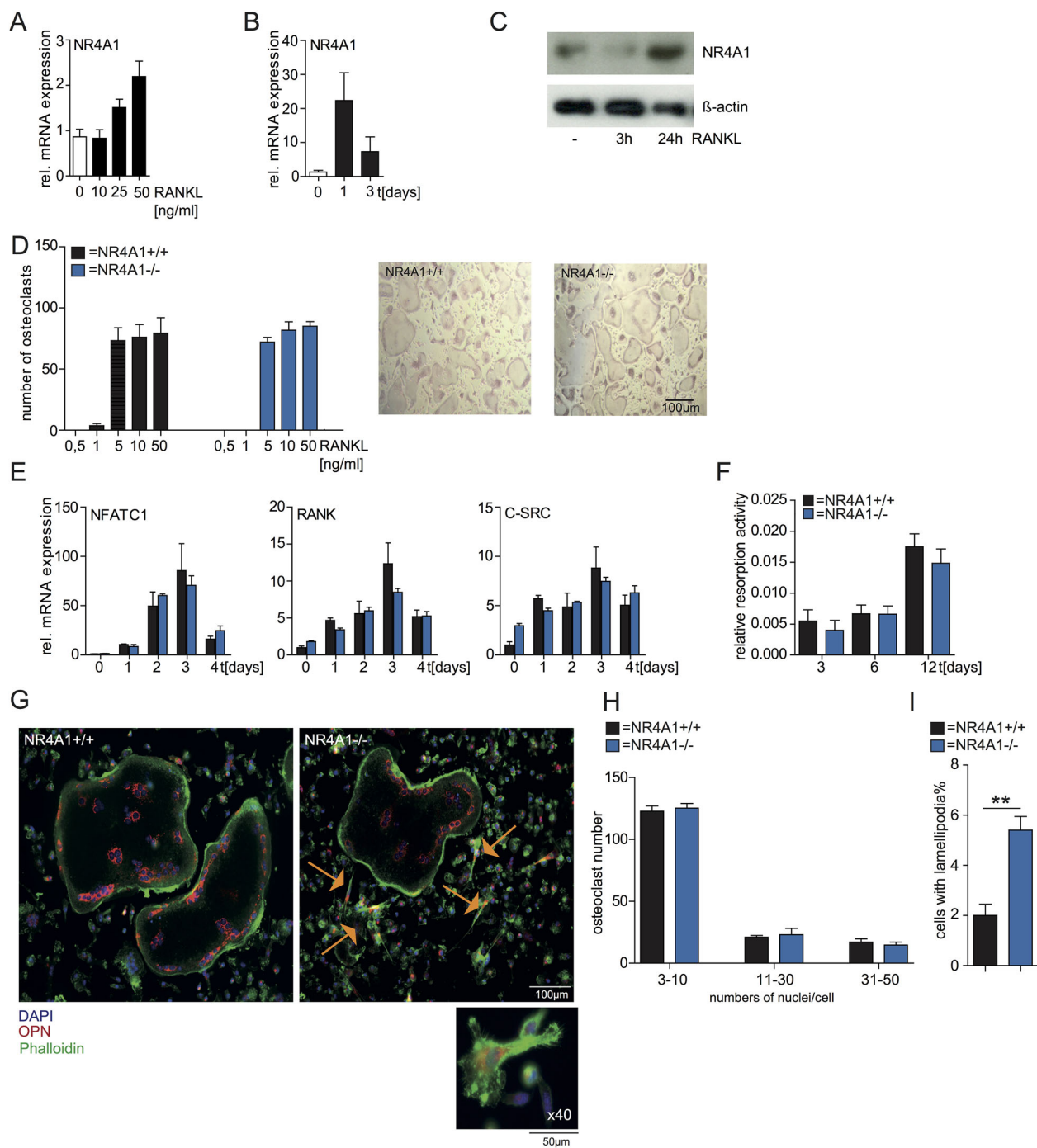


**Fig. 3.** Differentiation, fusion, and resorption are unaffected in NR4A1<sup>-/-</sup> osteoclasts. (A) Quantitative RT-PCR for determination of relative mRNA levels of NR4A1 normalized on  $\beta$ -actin after 2 hours' stimulation of osteoclast precursors with indicated RANKL concentrations. (B) Quantitative RT-PCR for relative mRNA levels of NR4A1 normalized on  $\beta$ -actin after stimulation of osteoclast precursors with RANKL (10 ng/mL) for indicated time points. (C) Western blot analysis of wild-type osteoclast precursors after stimulation with RANKL (10 ng/mL) at indicated time points. (D) Quantification and representative images of the TRAP-stained wild-type and NR4A1<sup>-/-</sup> osteoclasts on day 3 of osteoclast culture. Mature osteoclasts were identified as multinucleated TRAP<sup>+</sup> (purple) cells on day 3. (E) Expression of osteoclast-related genes in wild-type and NR4A1<sup>-/-</sup> osteoclasts after stimulation of osteoclast precursors with RANKL (10 ng/mL) for indicated time points. (F) Quantification of osteoclast-mediated resorption via measurement of calcium release from bone plates into culture medium at different days of osteoclast culture. (G) Immunofluorescence images of wild-type and NR4A1<sup>-/-</sup> osteoclasts during fusion on day 3 after RANKL-induced osteoclast differentiation. To visualize cell fusion and cytoskeletal characteristics, cells were incubated with antibodies against osteopontin (OPN in red), phalloidin (in green), and DAPI (in blue). (H) Quantification of the distribution of nuclei number per cell (= fusion events). (I) The cells with the presence of lamellipodia were counted and set in ratio to round cells per area.

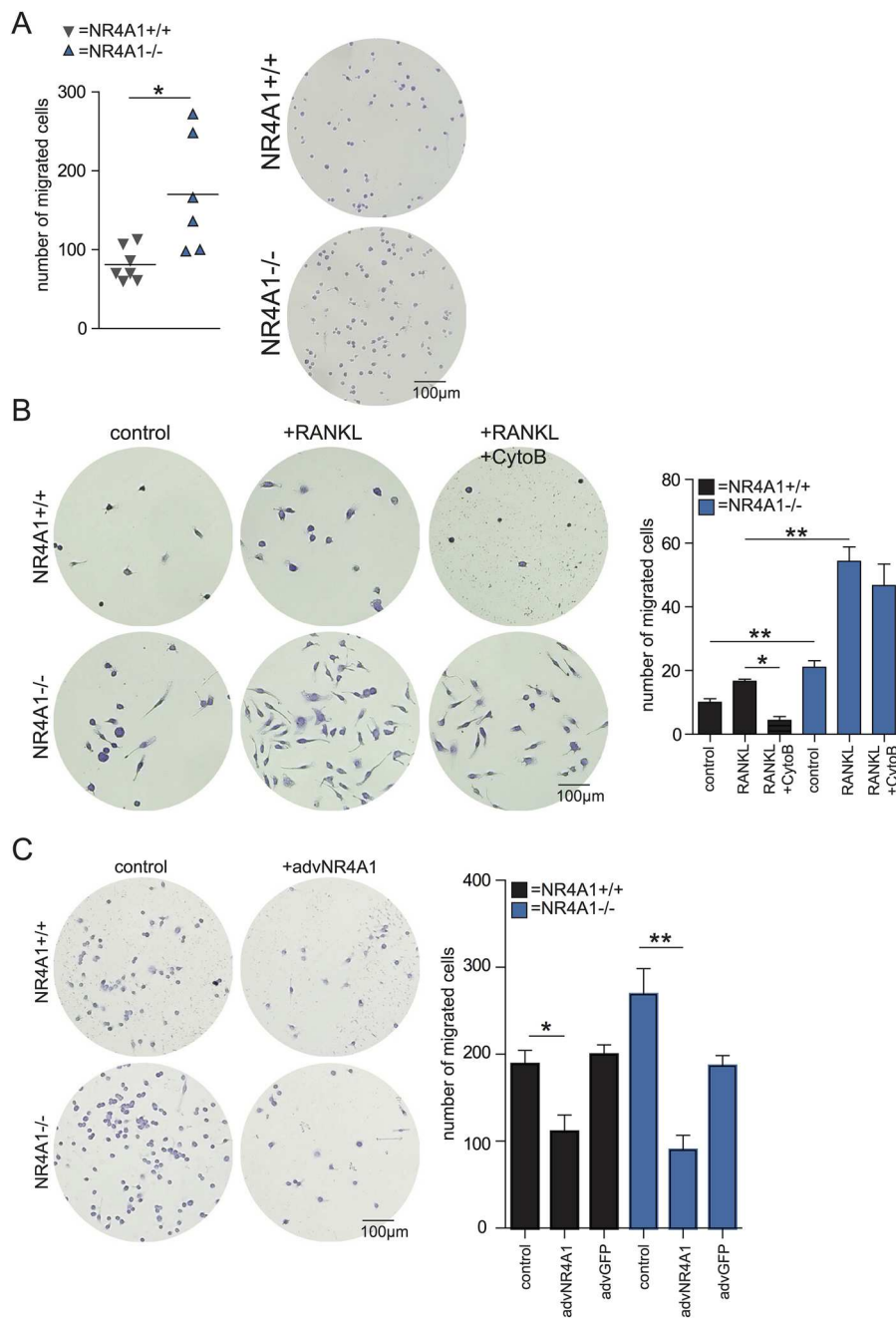


**Fig. 4.** NR4A1 regulates migration of osteoclast precursors. (A) Transwell assays showing numbers of migrated wild-type and NR4A1<sup>-/-</sup> osteoclast precursors (stained with crystal violet) that reached the lower part of the filter membrane (8-µm pore size) after 8 hours. (B) Wild-type and NR4A1<sup>-/-</sup> osteoclast precursors were subjected to in vitro scratch assays with images captured at 24 hours after stimulation with RANKL (10 ng/mL) and Cytosporone B (CytoB; 5 µM). Cells were stained with crystal violet and migrated cells into the scratched area were counted. (C) In vitro scratch assay with NR4A1 adenovirus (advNR4A1) or GFP adenovirus (advGFP = control) transduced wild-type and NR4A1<sup>-/-</sup> osteoclast (stained with crystal violet) precursors after 24 hours.

monocytes, OCPs, osteoclasts, and bone marrow-derived macrophages of wild-type and NR4A1<sup>-/-</sup> mice. Here, we focused on genes previously implicated in migration and motility of myeloid cells. This analysis showed that NR4A1-deficient cells displayed increased expression of multiple genes that had been previously implicated in cell migration and adhesion at different stages of osteoclastogenesis, suggesting that NR4A1 acted as transcriptional repressor of the motility of these cells. Such genes that were

regulated by NR4A1 included Rac1, Rac2, and CD44, as well as chemokine receptors such as CXCR4 (Supplemental Fig. S3). Osteopontin (OPN), a protein that has been recently described as a critical autocrine factor in the control of the motility of myeloid cells and of OC-mediated bone remodeling,<sup>(26,27)</sup> was the most prominently induced gene and dramatically upregulated in NR4A1<sup>-/-</sup> cells (>100 fold) (Fig. 5A). Moreover, Western blot-based analyses showed that OPN protein expression was

increased in absence of NR4A1 (Fig. 5B). Flow cytometry analysis of OCPs in blood, spleen, and bone marrow of wild-type and NR4A1<sup>-/-</sup> mice revealed no difference in CD44 expression, excluding an altered CD44-mediated adhesion potential of NR4A1<sup>-/-</sup> OCPs (Supplemental Fig. S4). However, we could confirm increased expression levels of OPN mRNA in the bone marrow of NR4A1<sup>fl/fl</sup>LysMCre(+/-) mice (Fig. 5C), which also showed elevated serum levels of OPN protein (Fig. 5D). Notably, analysis of the OPN promoter revealed multiple putative NR4A1 binding sites and chromatin immunoprecipitation experiments

confirmed specific binding of NR4A1 to these responsive elements in OCPs (Fig. 5E), suggesting a direct transcriptional control of OPN expression by this NR. This increased OPN expression in NR4A1<sup>fl/fl</sup>LysMCre(+/-) mice and OCPs prompted us to hypothesize that NR4A1 restricts OCP migration via negative regulation of OPN expression.

Consequently, we performed additional in vitro scratch assays to determine whether the NR4A1-mediated control of OCP migration was indeed mediated via regulation of OPN expression. The experiments confirmed an increased migration of

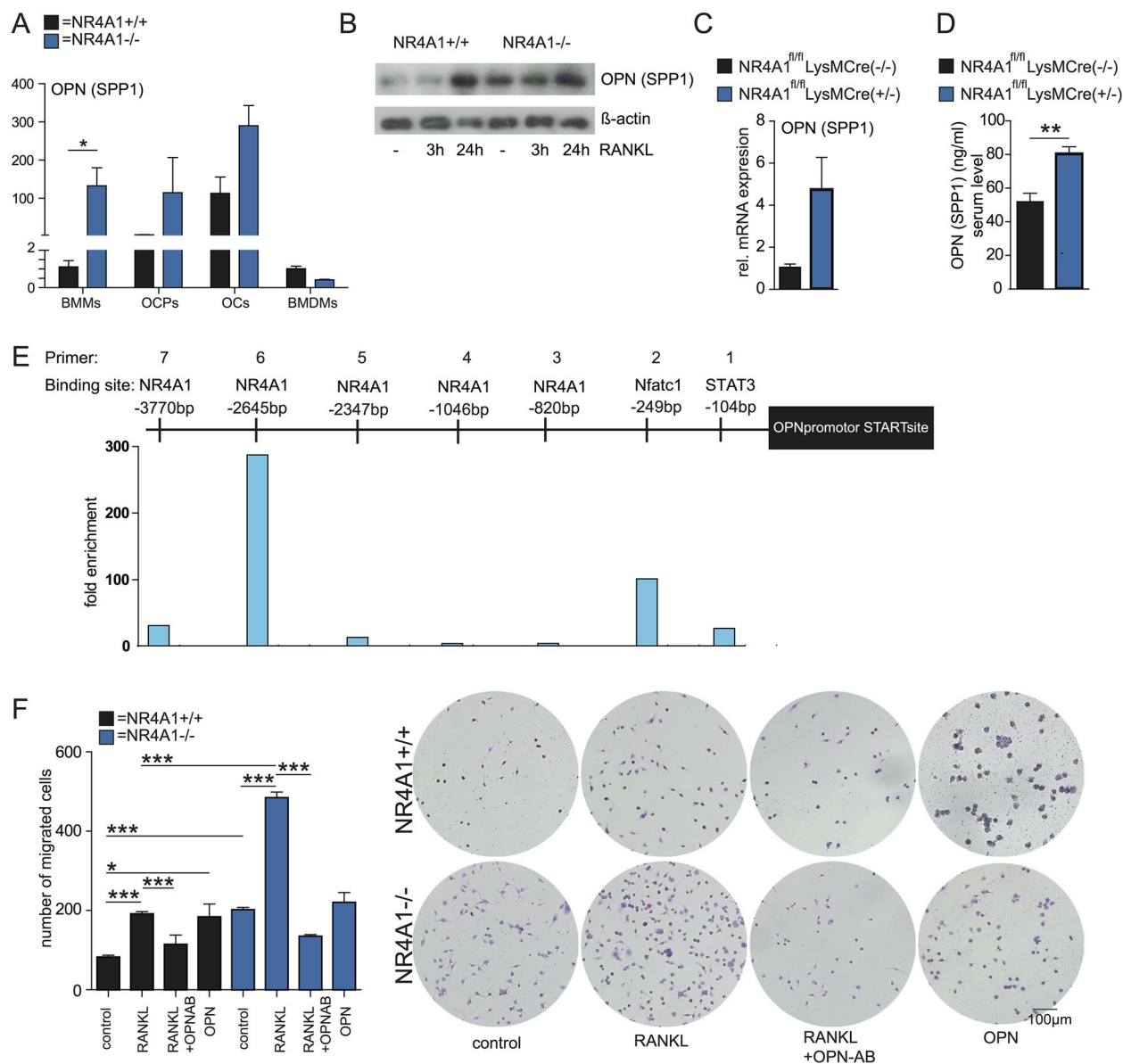


**Fig. 5.** NR4A1 governs migration of osteoclast precursors via OPN. (A) Quantitative RT-PCR for relative mRNA levels of osteopontin (OPN = SPP1) normalized on  $\beta$ -actin in wild-type and NR4A1<sup>-/-</sup> bone marrow-derived monocytes (BMMs), osteoclast precursors (OCPs), mature osteoclasts (OCs), and bone marrow-derived macrophages (BMDMs). (B) Western blot analysis of wild-type NR4A1<sup>+/+</sup> and NR4A1<sup>-/-</sup> osteoclast precursors after stimulation with RANKL (10 ng/mL) at indicated time points. (C) Quantitative RT-PCR for relative mRNA levels of osteopontin (OPN = SPP1) normalized on  $\beta$ -actin in BMMs from NR4A1<sup>fl/fl</sup>LysMCre(+/-) and wild-type littermates. (D) ELISA-based quantifications of OPN serum levels from female NR4A1<sup>fl/fl</sup>LysMCre(+/-) and wild-type littermates at 12 weeks of age. (E) Analysis of binding of NR4A1 to different regions of the mouse OPN promoter by chromatin immunoprecipitation in osteoclast precursors. (F) Wild-type and NR4A1<sup>-/-</sup> osteoclast precursors were subjected to in vitro scratch assay with images captured at 24 hours after stimulation with RANKL (10 ng/mL), soluble OPN (100  $\mu$ g/mL), and OPN-specific antibody (OPN-AB; 5  $\mu$ g). Cells were stained with crystal violet and migrated cells into the scratched area were counted.

NR4A1<sup>-/-</sup> OCPs compared with wild-type cells and amelioration of OCP migration administering an OPN antibody in wild-type and particularly in NR4A1<sup>-/-</sup> OCPs (Fig. 5F). OPN administration, in turn, increased wild-type OCP migration in the absence of RANKL, whereas no additional effect could be detected in NR4A1<sup>-/-</sup> OCPs. These data were in accordance with an NR4A1-mediated control of OCP migration that was largely dependent on the regulation of OPN expression.

### Pharmacological activation of NR4A1 rescues mice from OVX-induced bone loss

Postmenopausal osteoporosis is the most common cause of osteoporosis in humans and characterized by an increased osteoclast-mediated bone resorption.<sup>(3)</sup> OPN was recently described as a biomarker for the early diagnosis of osteoporosis in postmenopausal women.<sup>(28)</sup> Having identified NR4A1 as a novel regulator of OPN expression and OCP motility, we evaluated its potential as a therapeutic target during the OVX-induced model of postmenopausal bone loss. OVX was performed with female mice at an age of 12 weeks. NR4A1 mRNA or protein expression in osteoblasts or osteoclasts did not significantly change upon OVX (Supplemental Fig. S5A, B). Daily treatment with the NR4A1 agonist CytoB started after the onset of osteoporosis (2 weeks after surgery) for additional 6 weeks (Fig. 6A). ELISA-based quantification confirmed that CytoB treatment indeed blocked the OVX-induced increase in serum OPN levels (Fig. 6B) and ameliorated OVX-induced bone resorption activity (Fig. 6C), which was accompanied by an inhibition of the excessive OC formation at the trabecular bone surface that followed OVX (Fig. 6D). In line with these findings,  $\mu$ CT analysis confirmed a complete rescue of OVX-induced bone loss after CytoB treatment (Fig. 6E). Notably, CytoB treatment had no impact on bone homeostasis during the steady state in sham-operated mice.

## Discussion

Here, we identified the nuclear receptor NR4A1 as novel regulator of the motility of OCPs, resulting in increased OC-mediated bone resorption and reduced trabecular numbers in NR4A1-deficient mice. Notably, cortical thickness was not affected, which is in line with the fact that pathologically and enhanced OC-mediated bone turnover during diseases such as postmenopausal osteoporosis also primarily affects trabecular bone.<sup>(1)</sup> Although the process of OC differentiation and fusion has been extensively studied, little is known about specific pathways and molecules that control the recruitment and mobility of OCPs. The limited knowledge on OCP recruitment is partially owing to the fact that OCPs are less well defined than precursors of other myeloid lineages such as macrophages or dendritic cells. Among monocyte subsets, Ly6C<sup>high</sup> monocytes were shown to display the highest osteoclastogenic potential, whereas Ly6C<sup>low</sup> monocytes do not seem to differentiate into OCs to a similar extent.<sup>(29)</sup> Notably, NR4A1-deficient mice were shown to specifically lack Ly6C<sup>low</sup> monocytes in their peripheral blood.<sup>(18)</sup> However, because myeloid-specific deletion of NR4A1 did not result in a similar phenotype (Supplemental Fig. S6), this altered monocyte composition is unlikely to contribute to the currently observed bone phenotype.

Most of our knowledge on the migratory activity of myeloid cells is derived from studies focusing on macrophages. Here, surface molecules, including integrins and CD44 as well as intracellular

cytoskeleton-associated proteins such as RAC, are known to promote motility.<sup>(30–32)</sup> Monocytes and OCPs are considered to recirculate between bone marrow and the periphery. OCPs were reported to guide toward bone surfaces via the action of sphingosine 1-phosphate receptors (S1PRs) and EB12 receptor signaling.<sup>(33,34)</sup> However, the intracellular signals that regulate this OCP movement toward bone surfaces remain unknown.

Our data suggest an important role of NR4A1 as regulator of OPN-mediated OCP migration. Although other NR4A1-regulated genes might contribute to the migratory phenotype of NR4A1-deficient OCPs, our findings suggest a major role of OPN during the observed phenotype. Although our *in vitro* and *in vivo* data strongly suggest an intrinsic role of NR4A1 in OCs and/or OCPs, we cannot formally exclude that macrophages contribute to the observed bone phenotype in NR4A1<sup>fl/fl</sup>LysMCre(+/-) mice. The NR4A1-mediated regulation of OPN is of particular interest, as OPN is a well-known regulator of OC migration.<sup>(26,35)</sup> OPN is highly expressed in both osteoblasts and osteoclasts and is upregulated during bone turnover and skeletal remodeling.<sup>(36,37)</sup> Meanwhile, we know that OPN is expressed by various cells of the innate immune system and that it additionally acts as a cytokine with both pro-inflammatory and anti-inflammatory properties.<sup>(38–40)</sup> OPN has been shown to regulate T-cell activation, leukocyte recruitment, as well as cell migration<sup>(41–43)</sup> and has been implicated in the pathogenesis of different inflammatory and autoimmune diseases<sup>(44,45)</sup> as well as a factor affecting tumorigenesis.<sup>(46,47)</sup> Initially, OPN has been described as a molecule expressed in osteoblasts, where it accumulates in mineralized bone matrix. Substrate-bound OPN anchors osteoclasts to bone tissue by binding its receptor Itgb3 on the osteoclast cell surface.<sup>(48)</sup> In recent years, multiple studies have demonstrated that OCs can also express the message for OPN and suggested that OCPs could be a major source of OPN.<sup>(49)</sup> Recently, it has been shown that osteoclasts secrete OPN from their basolateral cell membranes as an autocrine motility factor to stimulate cell shape changes and cytoskeletal rearrangement to enable migration and bone resorption.<sup>(27)</sup> However, the exact underlying molecular mechanisms are incompletely understood. Notably, increased OPN levels were reported to be associated with low bone mineral density in postmenopausal women,<sup>(28,50)</sup> and mice lacking OPN were reported to be resistant to ovariectomy-induced bone loss,<sup>(51)</sup> suggesting a potential contribution of OPN to OC-mediated bone loss during postmenopausal bone loss in mice and humans. Like other nuclear receptors, members of the NR4A family were shown to act both as transcriptional activators and repressors. This dual way of action is linked to their potential to recruit transcriptional co-activators and co-repressors, respectively,<sup>(52–54)</sup> as well as to their phosphorylation status.<sup>(53,55)</sup> Our data suggest that NR4A1 indeed acts as negative regulator of OPN expression. It is not entirely clear why the increased OPN-mediated motility of NR4A1-deficient osteoclasts results in enhanced bone resorption *in vivo* but not *in vitro*. However, these findings are in accordance with the observed phenotype of OPN-deficient mice, which show protection from ovariectomy-induced osteoclastogenesis and bone loss *in vivo*, whereas *in vitro* osteoclastogenesis and resorption is not impaired but increased.<sup>(51,56)</sup>

Another recent study has suggested an additional role of NR4A1 in OC differentiation.<sup>(20)</sup> The authors showed that a global deficiency in NR4A1 results in increased numbers of OCs and osteopenia. Experiments with bone marrow chimeras indicated that this phenotype is linked to NR4A1 expression

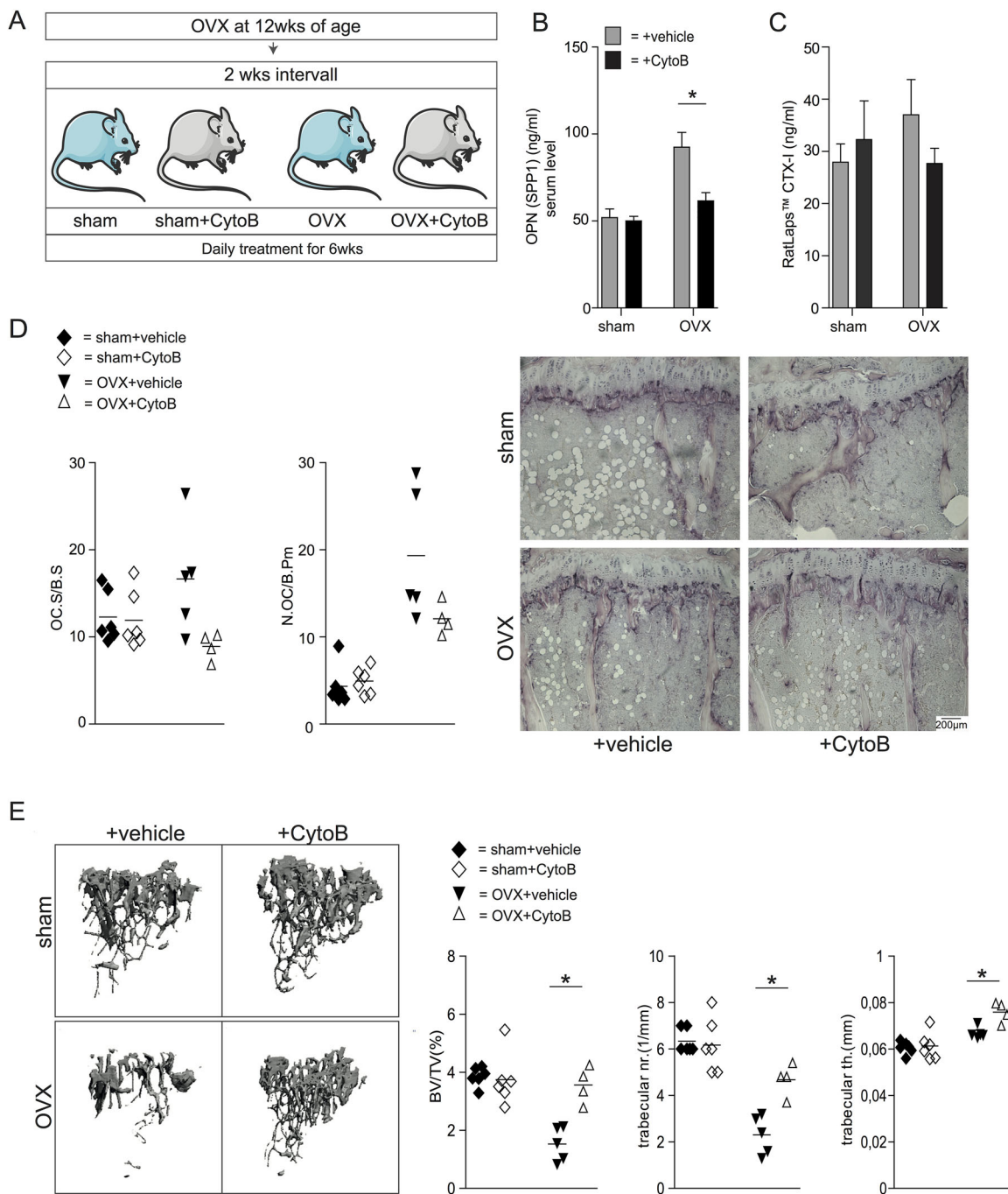


**Fig. 6.** NR4A1 protects from ovariectomy-induced bone loss. (A) Experimental setting for the postmenopausal mouse model of ovariectomy-induced bone loss and treatment strategy. (B) OPN and (C) bone-related degradation products (RatLaps; CTX-I) serum levels in ovariectomized (OVX) and sham-operated female mice after 6 weeks' treatment with Cyclosporine B (10 mg/kg body weight). (D) Histomorphometric analysis by TRAP staining determining the number of osteoclasts per bone surface (OC.S/B.S) and the percentage of surface covered by osteoclasts (N.OC/B.Pm) in ovariectomized and sham-operated mice after treatment with Cyclosporine B (CytoB). (E)  $\mu$ CT images and assessment of parameters of bone microarchitecture, including bone volume to total volume (BV/TV), trabecular number (trabecular nr.), and trabecular thickness (trabecular th.) in ovariectomized (OVX) or sham-operated animals after treatment with the NR4A1-specific agonist CytoB or a vehicle (DMSO), respectively. Significance of CytoB treatment efficiency was calculated by using Mann-Whitney *U* test.

in bone marrow-derived cells, which would include myeloid and lymphoid cells. Our current data using Runx2-Cre- and LysM-Cre-mediated conditional deletion of NR4A1 largely confirm these findings and additionally reveal that myeloid-specific deletion of

this nuclear receptor results in increased OC numbers. In contrast to the study by Li and colleagues,<sup>(20)</sup> however, we did not observe any direct effect of NR4A1 on Nfatc1 expression or the differentiation of OCs, but rather an impact on the migration

of OCPs. Although the reason for this discrepancy is not entirely clear, both studies support an important role of NR4A1 in OC biology. These insights highlight this nuclear receptor as potential target during the treatment of diseases that are linked to an exacerbated OC recruitment and differentiation. Our current study further shows that ligand-induced activation of this nuclear receptor interferes with the migratory activity of OCPs and exerts a bone-protective effect in the OVX model of postmenopausal osteoporosis, thus providing a first proof of concept that the blockade of OCP recruitment might be a feasible approach to treat OC-mediated diseases such as osteoporosis.

## Disclosures

All authors state that they have no conflicts of interest.

## Acknowledgments

This study was supported by the Deutsche Forschungsgemeinschaft (SPP1468-IMMUNOBONE and CRC1181 to GK, GS, and JT), the emerging field initiative (EFI) of the University Erlangen-Nürnberg, the Interdisciplinary Centre for Clinical Research, Erlangen (IZKF J48 to CS, A55 to GK, and A68 to GK and FN), the BMBF (METARTHROS to GK and GS), the Else-Kröner Fresenius Stiftung (2013\_A274 to GK). The work was further supported by the Collaborative Research Centre 1149 'Trauma' (INST 40/492-1). Vectors encoding for murine Rcor1, Rcor2, and Rcor3 were donated by S Saleque (Department of Biology, City College of New York and Graduate Center of City University of New York, New York, NY, USA). The vector pGL4.10[luc2] was kindly provided by Dr J Wittmann, Division of Molecular Immunology, University of Erlangen, Germany.

Authors' roles: CS designed the study, performed experiments, interpreted data, and wrote the first draft of the manuscript. NI, CB, BK, MS, TC, KP-Z, and TR designed and performed experiments and interpreted data. DW, AK and CS helped with technical support. JD, MH, JT, and GS helped to design the study and provided important technical input and mice. GK designed the study and wrote the manuscript. All authors read and commented on the manuscript.

## References

- Zaidi M. Skeletal remodeling in health and disease. *Nat Med.* 2007;13(7):791–801.
- Oursler MJ. Recent advances in understanding the mechanisms of osteoclast precursor fusion. *J Cell Biochem.* 2010;110(5):1058–62.
- Teitelbaum SL. Bone resorption by osteoclasts. *Science.* 2000;289(5484): 1504–8.
- Pei L, Waki H, Vaitheesvaran B, Wilpitz DC, Kurland IJ, Tontonoz P. NR4A orphan nuclear receptors are transcriptional regulators of hepatic glucose metabolism. *Nat Med.* 2006;12(9):1048–55.
- Desvergne B, Wahli W. Peroxisome proliferator-activated receptors: nuclear control of metabolism. *Endocr Rev.* 1999;20(5):649–88.
- Ipseiz N, Scholtysek C, Culemann S, Kronke G. Adopted orphans as regulators of inflammation, immunity and skeletal homeostasis. *Swiss Med Wkly.* 2014;144:w14055.
- Ipseiz N, Uderhardt S, Scholtysek C, et al. The nuclear receptor Nr4a1 mediates anti-inflammatory effects of apoptotic cells. *J Immunol.* 2014;192(10):4852–8.
- Kleyer A, Scholtysek C, Bottesch E, et al. Liver X receptors orchestrate osteoblast/osteoclast crosstalk and counteract pathologic bone loss. *J Bone Miner Res.* 2012;27(12):2442–51.
- Scholtysek C, Katzenbeisser J, Fu H, et al. PPARbeta/delta governs Wnt signaling and bone turnover. *Nat Med.* 2013;19(5):608–13.
- Imai Y, Kondoh S, Kouzmenko A, Kato S. Regulation of bone metabolism by nuclear receptors. *Mol Cell Endocrinol.* 2009;310(1–2):3–10.
- Wei W, Wang X, Yang M, et al. PGC1beta mediates PPARgamma activation of osteoclastogenesis and rosiglitazone-induced bone loss. *Cell Metab.* 2010;11(6):503–16.
- Wan Y, Chong LW, Evans RM. PPAR-gamma regulates osteoclastogenesis in mice. *Nat Med.* 2007;13(12):1496–503.
- Martinez-Gonzalez J, Badimon L. The NR4A subfamily of nuclear receptors: new early genes regulated by growth factors in vascular cells. *Cardiovasc Res.* 2005;65(3):609–18.
- Pei L, Castrillo A, Chen M, Hoffmann A, Tontonoz P. Induction of NR4A orphan nuclear receptor expression in macrophages in response to inflammatory stimuli. *J Biol Chem.* 2005;280(32):29256–62.
- Zhao Y, Bruemmer D. NR4A orphan nuclear receptors: transcriptional regulators of gene expression in metabolism and vascular biology. *Arterioscler Thromb Vasc Biol.* 2010;30(8):1535–41.
- Chen Y, Wu R, Chen HZ, et al. Enhancement of hypothalamic STAT3 acetylation by nuclear receptor Nur77 dictates leptin sensitivity. *Diabetes.* 2015;64(6):2069–81.
- Tontonoz P, Cortez-Toledo O, Wroblewski K, et al. The orphan nuclear receptor Nur77 is a determinant of myofiber size and muscle mass in mice. *Mol Cell Biol.* 2015;35(7):1125–38.
- Hanna RN, Carlin LM, Hubbeling HG, et al. The transcription factor NR4A1 (Nur77) controls bone marrow differentiation and the survival of Ly6C-monocytes. *Nat Immunol.* 2011;12(8):778–85.
- Tacke R, Hilgendorf I, Garner H, et al. The transcription factor NR4A1 is essential for the development of a novel macrophage subset in the thymus. *Sci Rep.* 2015;5:10055.
- Li X, Wei W, Huynh H, Zuo H, Wang X, Wan Y. Nur77 prevents excessive osteoclastogenesis by inducing ubiquitin ligase Cbl-b to mediate NFATc1 self-limitation. *Elife.* 2015;4:e07217.
- Liang CC, Park AY, Guan JL. In vitro scratch assay: a convenient and inexpensive method for analysis of cell migration in vitro. *Nat Protoc.* 2007;2(2):329–33.
- Kronke G, Bochkov VN, Huber J, et al. Oxidized phospholipids induce expression of human heme oxygenase-1 involving activation of cAMP-responsive element-binding protein. *J Biol Chem.* 2003;278(51): 51006–14.
- Rauch A, Seitz S, Baschant U, et al. Glucocorticoids suppress bone formation by attenuating osteoblast differentiation via the monomeric glucocorticoid receptor. *Cell Metab.* 2010;11(6):517–31.
- Clausen BE, Burkhardt C, Reith W, Renkawitz R, Forster I. Conditional gene targeting in macrophages and granulocytes using LysMcre mice. *Transgenic Res.* 1999;8(4):265–77.
- Zhan Y, Du X, Chen H, et al. Cyclosporine B is an agonist for nuclear orphan receptor Nur77. *Nat Chem Biol.* 2008;4(9):548–56.
- Standal T, Borset M, Sundan A. Role of osteopontin in adhesion, migration, cell survival and bone remodeling. *Exp Oncol.* 2004;26(3): 179–84.
- Chellaiah MA, Kizer N, Biswas R, et al. Osteopontin deficiency produces osteoclast dysfunction due to reduced CD44 surface expression. *Mol Biol Cell.* 2003;14(1):173–89.
- Chang IC, Chiang TI, Yeh KT, Lee H, Cheng YW. Increased serum osteopontin is a risk factor for osteoporosis in menopausal women. *Osteoporos Int.* 2010;21(8):1401–9.
- Seeling M, Hillenhoff U, David JP, et al. Inflammatory monocytes and Fc gamma receptor IV on osteoclasts are critical for bone destruction during inflammatory arthritis in mice. *Proc Natl Acad Sci U S A.* 2013;110(26):10729–34.
- Suzuki K, Zhu B, Rittling SR, et al. Colocalization of intracellular osteopontin with CD44 is associated with migration, cell fusion, and resorption in osteoclasts. *J Bone Miner Res.* 2002;17(8):1486–97.
- Huttenlocher A, Horwitz AR. Integrins in cell migration. *Cold Spring Harb Perspect Biol.* 2011;3(9):a005074.
- Allen WE, Jones GE, Pollard JW, Ridley AJ. Rho, Rac and Cdc42 regulate actin organization and cell adhesion in macrophages. *J Cell Sci.* 1997;110(Pt 6):707–20.

33. Ishii M, Egan JG, Klauschen F, et al. Sphingosine-1-phosphate mobilizes osteoclast precursors and regulates bone homeostasis. *Nature*. 2009;458(7237):524–8.
34. Nevius E, Pinho F, Dhodapkar M, et al. Oxysterols and EB12 promote osteoclast precursor migration to bone surfaces and regulate bone mass homeostasis. *J Exp Med*. 2015;212(11):1931–46.
35. Chellaiah MA, Hruska KA. The integrin alpha(v)beta(3) and CD44 regulate the actions of osteopontin on osteoclast motility. *Calcif Tissue Int*. 2003;72(3):197–205.
36. Denhardt DT, Noda M. Osteopontin expression and function: role in bone remodeling. *J Cell Biochem Suppl*. 1998;30–31:92–102.
37. Merry K, Dodds R, Littlewood A, Gowen M. Expression of osteopontin mRNA by osteoclasts and osteoblasts in modelling adult human bone. *J Cell Sci*. 1993;104(Pt 4):1013–20.
38. Mazzali M, Kipari T, Ophascharoensuk V, Wesson JA, Johnson R, Hughes J. Osteopontin—a molecule for all seasons. *QJM*. 2002;95(1):3–13.
39. Rittling SR. Osteopontin in macrophage function. *Expert Rev Mol Med*. 2011;13:e15.
40. Gravallesse EM. Osteopontin: a bridge between bone and the immune system. *J Clin Invest*. 2003;112(2):147–9.
41. Stromnes IM, Gorman JM. Osteopontin-induced survival of T cells. *Nat Immunol*. 2007;8(1):19–20.
42. Poggio P, Grau JB, Field BC, et al. Osteopontin controls endothelial cell migration in vitro and in excised human valvular tissue from patients with calcific aortic stenosis and controls. *J Cell Physiol*. 2011;226(8):2139–49.
43. Yue TL, McKenna PJ, Ohlstein EH, et al. Osteopontin-stimulated vascular smooth muscle cell migration is mediated by beta 3 integrin. *Exp Cell Res*. 1994;214(2):459–64.
44. Jansson M, Panoutsakopoulou V, Baker J, Klein L, Cantor H. Cutting edge: attenuated experimental autoimmune encephalomyelitis in eta-1/osteopontin-deficient mice. *J Immunol*. 2002;168(5):2096–9.
45. Petrow PK, Hummel KM, Schedel J, et al. Expression of osteopontin messenger RNA and protein in rheumatoid arthritis: effects of osteopontin on the release of collagenase 1 from articular chondrocytes and synovial fibroblasts. *Arthritis Rheum*. 2000;43(7):1597–605.
46. Raja R, Kale S, Thorat D, et al. Hypoxia-driven osteopontin contributes to breast tumor growth through modulation of HIF1alpha-mediated VEGF-dependent angiogenesis. *Oncogene*. 2014;33(16):2053–64.
47. Takafuji V, Forgues M, Unsworth E, Goldsmith P, Wang XW. An osteopontin fragment is essential for tumor cell invasion in hepatocellular carcinoma. *Oncogene*. 2007;26(44):6361–71.
48. Reinholt FP, Hulthén K, Oldberg A, Heinegård D. Osteopontin—a possible anchor of osteoclasts to bone. *Proc Natl Acad Sci U S A*. 1990;87(12):4473–5.
49. Dodds RA, et al. Human osteoclasts, not osteoblasts, deposit osteopontin onto resorption surfaces: an in vitro and ex vivo study of remodeling bone. *J Bone Miner Res*. 1995;10(11):1666–80.
50. Wei QS, Huang L, Tan X, Chen ZQ, Chen SM, Deng WM. Serum osteopontin levels in relation to bone mineral density and bone turnover markers in postmenopausal women. *Scand J Clin Lab Invest*. 2016;76(1):33–9.
51. Yoshitake H, Rittling SR, Denhardt DT, Noda M. Osteopontin-deficient mice are resistant to ovariectomy-induced bone resorption. *Proc Natl Acad Sci U S A*. 1999;96(14):8156–60.
52. Shaked I, Hanna RN, Shaked H, et al. Transcription factor Nr4a1 couples sympathetic and inflammatory cues in CNS-recruited macrophages to limit neuroinflammation. *Nat Immunol*. 2015;16(12):1228–34.
53. Palumbo-Zerr K, Zerr P, Distler A, et al. Orphan nuclear receptor NR4A1 regulates transforming growth factor-beta signaling and fibrosis. *Nat Med*. 2015;21(2):150–8.
54. Wansa KD, Harris JM, Muscat GE. The activation function-1 domain of Nur77/NR4A1 mediates trans-activation, cell specificity, and coactivator recruitment. *J Biol Chem*. 2002;277(36):33001–11.
55. Wingate AD, Arthur JS. Post-translational control of Nur77. *Biochem Soc Trans*. 2006;34(Pt 6):1107–9.
56. Rittling SR, Matsumoto HN, McKee MD, et al. Mice lacking osteopontin show normal development and bone structure but display altered osteoclast formation in vitro. *J Bone Miner Res*. 1998;13(7):1101–11.